Coupling the turbulent flow with the solidification processes in OpenFOAM®

A. Vakhrushev[1], A. Ludwig[2], M. Wu[1, 2], Y. Tang[3], G. Hackl[3], G. Nitzl[4]

[1] Christian Doppler Laboratory for Advanced Process Simulation of Solidification and Melting, University of Leoben, A-8700 Leoben, Austria
[2] Simulation and Modeling of Metallurgical Processes, Department of Metallurgy, University of Leoben, A-8700 Leoben, Austria
[3] RHI AG, Technology Center, Standort Leoben, Magnesitstrasse 2, A-8700 Leoben, Austria
[4] RHI AG, 1100 Vienna, Wienerberstrasse 11, Austria

Abstract

A basic task of the coupling a turbulent flow with the solidification processes during the numerical modeling is taken into account. A number of the convectional schemes been implemented in the OpenFOAM® CFD software is studied with regard to the accuracy and the boundness of the obtained numerical solution. The proper evaluation of the temperature field using unstructured numerical grid is considered. The segregated approach to treat the continuity, momentum and energy equations for the laminar incompressible liquid flow is compared with the fully-coupled PDE system solution. The sensitivity of the two-phase region growth to the permeability parameter variation is investigated along with the turbulent effect.

Keywords

Numerical modeling, solidification, multiphase flow, turbulence, OpenFOAM®

1. INTRODUCTION

It is well known that modeling of the solidification process is a rather complex task which includes the calculation of the heat transfer, fluid flow and phase transition. The multi-scale nature of the solidification problem increases the complexity of the numerical model (Fig. 1). On the one hand, taking the continuous casting as an example, the calculation domain spans a characteristic length scale of meters. The typical flow regime varies from the highly turbulent in the core and near the melt injection (e.g. at the ports of the submerged entry nozzle) regions to the laminar sublayer in the vicinity of the wall surfaces. On the other hand, the solid phase grows from the chilled wall, forming initially a two phase mushy zone which separates the fully-liquid core region from the fully-solidified shell. The two phase mushy zone consists of the solid dendrites at the length scale of ~100 micrometers and the interdendritic melt. The two phase region represents similarity of a porous medium, which is permeable for the flow. Additionally the solidified shell including the solid part of the mush is continuously pulled out of the casting mold that in turn influences the relative motion between the turbulent flow and the dendritic structures.

The progress of the solidification front is not pre-describable, and it is the result of interaction between the melt flow and the solidification. Remelting is often detected at the impingement point of the hot jet, which makes the shell profile non-uniform. Thereby the transient behavior of the solidification front along with the varying thickness of the two phase region requires special attention.

The preliminary studies [1] have shown the strong influence of the turbulence on the solidification process and vice-versa. Due to the mixing effect of the turbulence, the effective thermal conductivity increases significantly with the turbulence intensity, and this slows down the growth of the solid shell. On the other hand the dendritic mushy zone stabilizes the flow [2].

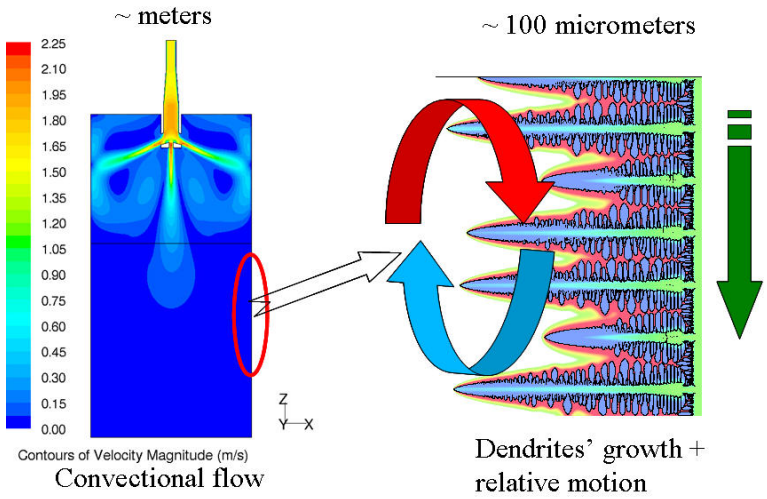

Figure 1. Multi-scale phenomenon of the solidification process

A number of numerical models, dealing with both fluid flow and heat transfer, and also incorporating the solidification kinetics, are known from the literature [3-4]. The earliest solidification models incorporated only the laminar flow [5-8]. The approaches for handling the turbulence during solidification were firstly reported in contributions [9-12]. Porous resistance of the two-phase region is combined with the heat transfer [1-2]. The current work includes a numerical model incorporating the turbulent flow with the mixture solidification model. The model is implemented in the CFD software package OpenFOAM®. Some improvements to the previous solidification model were made, and the numerical study and evaluation of the proper heat transfer simulation are presented.

2. MODELING TURBULENT FLOW AND SOLIDIFICATION

A number of approaches for modeling solidification were reviewed by Dantzig and Rappaz [13]. Different methods, which are widely used in the modern CFD field, either track all phases separately requiring exact interface position to be known or use an approach of fixed numerical grid along with an averaging of the physical properties of the considered phases. Here a fixed finite volume mesh is used with a collocated or non-staggered variable arrangement [14-15], where all physical values share the same control volumes (CV), and all flux variables reside on the CV faces. The divergence theorem is used throughout the discretization procedure. Unsteady formulation of the Navier-Stokes equations is used to track time-dependent process.

The following assumptions are made: the multiphase system is described as a viscous fluid with mixture properties [5-8]; the mixture continuum combines liquid (ℓ) phase and solid (s) phase (quantified by the corresponding volume fractions f_ℓ and f_s), which changes continuously from a pure liquid region, through the mushy zone (two phase region), to the complete solid region; the solidified shell along the mold walls morphologically represents the columnar phase (dendrites). The amount of the solid phase is determined with a solid

fraction-temperature curve. The steel slab is continuously pulled out with a pre-described pulling (casting) velocity $\vec{u}_{\text{pull}}$. The solid phase velocity $\vec{u}_s$ generally equals the pulling one for the conventional slab casting, but for the thin-slab mold with a complex geometry a surface curvature is to be taken into account.

The Navier-Stokes equations with an assumption of the liquid incompressibility are used to simulate the melt velocity. Only one set of equations is formulated for both phases in the Eulerian frame of the reference. The mixture velocity $\vec{u} = f_\ell \vec{u}_\ell + f_\text{s}\vec{u}_\text{s}$ represents a weighted sum of the liquid and solid velocities with the phase fractions as weighting factors. Thereby, the equation system consisting of the continuity and momentum equations is

$$\nabla \cdot \vec{u} = 0, \tag{1}$$

$$\rho \frac{\partial \vec{u}}{\partial t} + \rho \nabla \cdot (\vec{u}\,\vec{u}) = -\vec{\nabla} p + \nabla \cdot (\mu_{\text{eff}} \vec{\nabla} \vec{u}) + \vec{S}_\text{D}, \tag{2}$$

where μ_{eff} is the effective dynamic viscosity of the liquid, which includes laminar and turbulent parts and varies throughout the calculation domain due to the turbulence effect. The influence of the mush region on the flow is defined by the source tem $\vec{S}_\text{D}$ in the momentum equation (2) mirroring a drag force inside the porous region. The Blake-Kozeny law is used to model the porous resistance of the dendritic structures based on the relative velocity:

$$\vec{S}_\text{D} = -\frac{\mu_\ell}{K} \cdot (\vec{u} - \vec{u}_\text{s}), \tag{3}$$

where μ_ℓ is the laminar viscosity and $(\vec{u} - \vec{u}_\text{s})$ is the relative velocity of the mixture in the porous region. The permeability (K) of the mushy zone depends on the solid volume fraction and the characteristic length (the primary arm spacing λ_1 [16]) of the dendrites:

$$K = \frac{(1 - f_s)^3}{f_\text{s}^{\,2}} \cdot 6 \cdot 10^{-4} \cdot \lambda_1^2. \tag{4}$$

Prescribed f_s-T relations of different types (e.g. linear or Gulliver-Scheil) are used to track the evolution of the solid phase.

The complexity of the solidification model at the presence of the turbulence arises mostly from the flow regime transition from its fully-liquid core, through a liquid-solid two phase region, to a fully-solid region with a prescribed moving velocity. To deal with such problem a comprehensive model is employed to incorporate a description of the turbulent core along with a laminar sublayer and a "solid body" behavior for the limit case $f_\text{s} = 1$ using significant damping of the flow inside multiphase region. A RANS turbulence model is used based on a low Reynolds number $k - \varepsilon$ model, as introduced by Prescott and Incropera [9-12]:

$$\rho \frac{\partial k}{\partial t} + \rho \nabla \cdot (\vec{u} k) = \nabla \cdot \left(\left(\mu_\ell + \frac{\mu_\text{t}}{\text{Pr}_{\text{t,k}}} \right) \vec{\nabla} k \right) + G - \rho \varepsilon + S_\text{k}, \tag{5}$$

$$\rho \frac{\partial \varepsilon}{\partial t} + \rho \nabla \cdot (\vec{u} \varepsilon) = \nabla \cdot \left(\left(\mu_\ell + \frac{\mu_\text{t}}{\text{Pr}_{\text{t},\varepsilon}} \right) \vec{\nabla} \varepsilon \right) + C_{1\varepsilon} G \frac{\varepsilon}{k} - C_{2\varepsilon} \rho \frac{\varepsilon^2}{k} + S_\varepsilon, \tag{6}$$

$$S_{\mathrm{k}} = -\frac{\mu_\ell}{K}\cdot k\,,\quad S_\varepsilon = -\frac{\mu_\ell}{K}\cdot \varepsilon\,, \tag{7}$$

where $\mathrm{Pr}_{\mathrm{t,k}} = 1$, and $\mathrm{Pr}_{\mathrm{t},\varepsilon} = 1.3$ are the turbulent Prandtl numbers for k and ε, respectively; G is the shear production of turbulence kinetic energy [9-12]. A turbulence dumping mechanism is similar to that being used for the momentum equation (2) introducing a linear reduction of the turbulent parameters in the mush.

The evolution of the solid phase is calculated according to the temperature by solving the energy equation. The energy equation of the mixture columnar solidification applicable for the continuous casting (CC) can be derived from the Eulerian two-phase energy equations:

$$\frac{\partial}{\partial t}(f_l\rho_l h_l) + \nabla\cdot\left(f_l\rho_l\vec{u}h_l\right) = \nabla\cdot\left(\alpha_l f_l\vec{\nabla}T_l\right) + Q_{sl}\,, \tag{8}$$

$$\frac{\partial}{\partial t}(f_s\rho_s h_s) + \nabla\cdot\left(f_s\rho_s\vec{u}_s h_s\right) = \nabla\cdot\left(\alpha_s f_s\vec{\nabla}T_s\right) - Q_{sl}\,. \tag{9}$$

The liquid enthalpy h_l is defined

$$h_l = h_s + L\,, \tag{10}$$

where h_s, further denoted simply as h, is a sensitive enthalpy of the solid. L is the latent heat (heat of fusion), and the term Q_{sl} is the energy exchange rate between the solid and liquid. Due to the energy conservation condition, this term exists in both equations but with the opposite signs.

In the mixture solidification model both phases are assumed to have the same density, $\rho_l = \rho_s = \rho$, and same temperatures, $T_l = T_s = T$. Hereby, summing up equations (8) to (9) and employing enthalpy formulation (10), we obtain:

$$\rho\frac{\partial h}{\partial t} + \rho\nabla\cdot\left(\vec{u}h\right) + \rho L\frac{\partial f_l}{\partial t} + \rho L\nabla\cdot\left(f_l\vec{u}_l\right) = \nabla\cdot\left(\alpha\vec{\nabla}T\right). \tag{11}$$

In the reference of the mixture model the term $\nabla\cdot\left(f_l\vec{u}_l\right)$ is unknown in the transport equation (11) because the individual quantities of the solid and liquid are not considered and it is not possible to track them based on the simulation results. In spite of the specified intricacy it is possible to resolve the ambiguity in the denoted advection term $\nabla\cdot\left(f_l\vec{u}_l\right)$. Thereto one should employ the continuity equation (1) together with the definition of the mixture velocity ($\vec{u} = f_\ell\vec{u}_\ell + f_{\mathrm{s}}\vec{u}_{\mathrm{s}}$),

$$\nabla\cdot\left(f_l\vec{u}_l\right) = -\nabla\cdot\left(f_s\vec{u}_s\right). \tag{12}$$

The solid velocities are estimated based on the boundary conditions, assumed Young's modulus and the Poisson ratio of the considered material. In view of the fact $f_\ell + f_{\mathrm{s}} = 1$ and including the turbulence influence for the thermal conductivity $\alpha_{\mathrm{eff}} = \alpha_l + \alpha_t$, the final form of the energy equation (11) would be

$$\rho\frac{\partial h}{\partial t} + \rho\nabla\cdot\left(\vec{u}h\right) = \nabla\cdot\left(\alpha_{\mathrm{eff}}\nabla T\right) + \rho L\frac{\partial f_s}{\partial t} + \rho L\nabla\cdot\left(f_s\vec{u}_s\right). \tag{13}$$

Some numerical investigations have shown that a conservative form of the advective term is less preferable than a gradient one:

$$\rho\frac{\partial h}{\partial t}+\rho\nabla\cdot\left(\vec{u}h\right)=\nabla\cdot\left(\alpha_{\text{eff}}\vec{\nabla}T\right)+\rho L\frac{\partial f_s}{\partial t}+\rho L\vec{u}_s\vec{\nabla}f_s+\rho Lf_s\nabla\cdot\vec{u}_s. \tag{14}$$

If compared to the previous investigations [1-2, 17-18], latent heat source term is supplemented with the additional component $\rho Lf_s\nabla\cdot\vec{u}$ based on the divergence of the solid velocities. The latest exhibits when the curvature of the mold surface is significant and it is necessary to treat the complex geometries of the simulation domain boundary. The simplified form of the energy equation (14) for the constant solid velocity $\vec{u}_{\text{s}}=\vec{u}_{\text{pull}}$ for the case of the straight mold geometry is

$$\rho\frac{\partial h}{\partial t}+\rho\nabla\cdot\left(\vec{u}h\right)=\nabla\cdot\left(\alpha_{\text{eff}}\vec{\nabla}T\right)+\rho L\frac{\partial f_s}{\partial t}+\rho L\vec{u}_{\text{pull}}\vec{\nabla}f_s. \tag{15}$$

Governing equations of the mixture solidification model defined in the current section were employed to design a stand-along solidification solver using the OpenFOAM® CFD software package. The solver was verified based on the experimental data and results of the numerical simulations using different CFD software [19]. Relevant results for the real casting processes were reported in the previous contributions of the authors [17-18].

3. CONVERGENCE AND ACCURACY OF TURBULENT FLOW SIMULATION

The proper prediction of the flow pattern is invariably of the great importance for the solidification model. However, some issues concerning turbulent flow were detected during numerical simulation using designed solidification solver within the framework of OpenFOAM®. Therein a detailed description is presented.

A general flow pattern in the continuous casting (CC) is presented in Fig. 2 for the case of the standard OpenFOAM® transient turbulent solver being used for the second order of accuracy.

To visualize a characteristic flow regime in the casting mold, a flow type function is introduced:

$$\mathbf{\Lambda}=\frac{|\mathbf{D}|-|\mathbf{\Omega}|}{|\mathbf{D}|+|\mathbf{\Omega}|}, \tag{16}$$

where $\mathbf{D}=\frac{1}{2}\left(\vec{\nabla}\vec{u}+\left(\vec{\nabla}\vec{u}\right)^T\right)$ is the symmetric part and $\mathbf{\Omega}=\frac{1}{2}\left(\vec{\nabla}\vec{u}-\left(\vec{\nabla}\vec{u}\right)^T\right)$ is the skew part of the velocity gradient tensor. Based on the $\mathbf{\Lambda}$ value a flow regime is defined as

$$\mathbf{\Lambda}=\begin{cases}-1 & \text{rotational flow,}\\ 0 & \text{simple shear flow,}\\ 1 & \text{planar extentional flow.}\end{cases} \tag{17}$$

The solution is obtained with a strict convergence criterion setting the residuals value to the level of ~10^{-6}. In Fig. 2 (a)-(d) one can see the velocity field, turbulent kinetic energy, effective viscosity and flow type function, which specifies eddy structure of the flow.

At first sight simulation results seem satisfactory: a nice complex turbulent structure is resolved similar to those obtained with large eddy simulation (LES) method. However, in-depth analysis of the turbulent kinetic energy (Fig. 2 (b)) shows a failure of convergence.

Corresponding field seems to be “frozen” and does not vary with time. The cells with the highest turbulent energy are observed around the outlets of the SEN ports which fit to the unstructured grid location with the highly skewed elements due to the complexity of the calculation domain. These high values are not transported to the neighboring regions, thus k and ε parameters remain close to zero in the most regions. Thereby the turbulent viscosity is estimated as

$$\lim_{k,\varepsilon\to 0}\mu_t = \lim_{k,\varepsilon\to 0}\left(\rho C_\mu \frac{k^2}{\varepsilon}\right) = 0\,. \tag{18}$$

It is overall too low and, as the consequence, the effective viscosity μ_{eff} does not vary distinctly from the initial laminar viscosity (Fig. 2(c)). The described numerical error leads to the under-estimation of the mixing being typically observed for the turbulent flows.

Summarizing the above discussion, a highly resolved turbulent structure on the fairly poor numerical grid using RANS approach is the result of the miss-converged numerical procedure. In the following part of the section the symptoms are interpreted and a “remedy” is proposed.

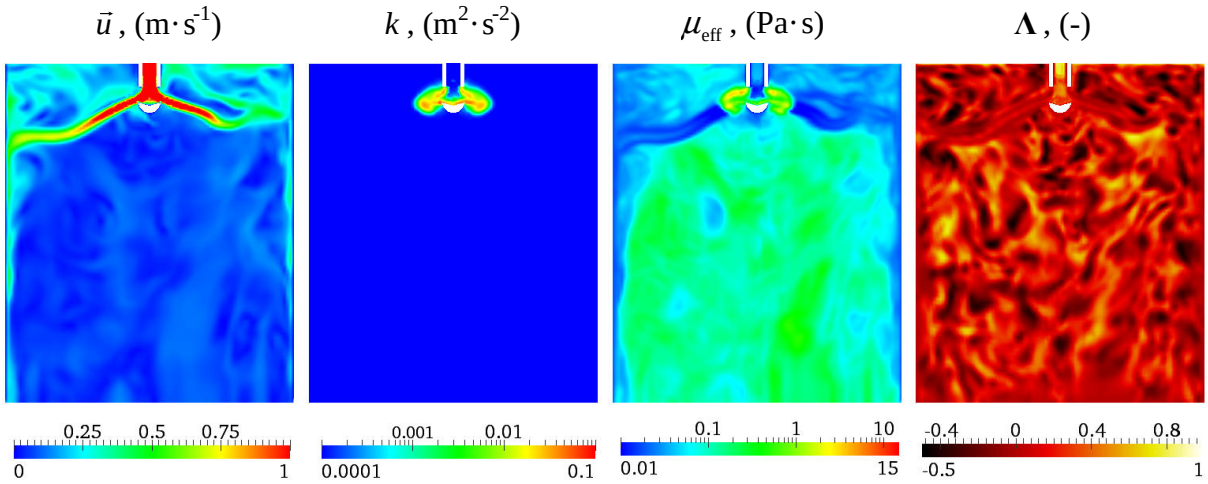

Figure 2. Flow pattern in the CC mold obtained with the *standard* solver:
(a) velocity field; (b) turbulent kinetic energy; (c) effective viscosity; (d) flow type function.

It was found that actually a source of the denoted failure resides in the residuals normalization procedure of the OpenFOAM®. The initial linear system of equations being solved after discretization procedure can be written as

$$\mathbf{A}\times\boldsymbol{\psi} = \mathbf{b} \tag{19}$$

$\boldsymbol{\psi} = \{\psi_i\}$ and $\mathbf{b} = \{b_i\}$ are n-sized vectors of scalars or tensors in accordance with the type of the field values to be calculated, $\mathbf{A} = \{a_{ij}\}$ is a scalar matrix (n × n). Currently the block matrix treatment is developed in the OpenFOAM to provide a full coupling between an arbitrary number of the partial differential equations (PDE).

Further let’s define

$$\boldsymbol{\Delta} = \mathbf{A}\times\boldsymbol{\psi}^*, \tag{20}$$

where $\boldsymbol{\psi}^*$ stands for the obtained numerical solution, then the matrix residual is

$$\mathbf{R} = \mathbf{b} - \boldsymbol{\Delta}. \tag{21}$$

It should be noted that $\mathbf{R}$ is actually a scalar or tensor vector with the number of elements $\{r_i\}$ equal to the number of the finite volume cells. Thereby, to estimate the overall error of the whole domain, residuals normalization with the normalization factor $\mathbf{N}$ is applied in OpenFOAM®:

$$\overline{\mathbf{R}} = \frac{1}{\mathbf{N}} \sum_{\text{all cells}} \|r_i\|. \tag{22}$$

The normalization factor $\mathbf{N}$ is calculated as

$$\mathbf{N} = \sum_{\text{all cells}} \left\{ \left\| \boldsymbol{\Delta} - \overline{\boldsymbol{\Delta}} \right\| + \left\| \mathbf{b} - \overline{\boldsymbol{\Delta}} \right\| \right\}, \tag{23}$$

where

$$\overline{\boldsymbol{\Delta}} = \overline{\mathbf{A}} \times \overline{\boldsymbol{\psi}}, \tag{24}$$

$$\overline{\mathbf{A}} = \sum_j a_{ij} = \begin{pmatrix} \sum a_{1j} \\ \sum a_{2j} \\ \vdots \\ \sum a_{nj} \end{pmatrix}, \tag{25}$$

$$\overline{\boldsymbol{\psi}} = \frac{1}{n} \sum_{i=1}^{n} \psi_i. \tag{26}$$

At the convergence of Eq. (17) the relationship of Eq. (21) can be reduced to the simple form

$$\mathbf{N} = 2 \sum_i \|b_i\|. \tag{27}$$

Thereby according to Eq. (27), normalization factor strongly depends on the source terms. Unstructured grid being exploited for the complex geometries introduces a huge amount of the non-orthogonality, which should be treated during gradient calculation when the high order convectional schemes are used. The common approach is based on the non-orthogonal correction procedure, which actually results in the additional source terms in the right-hand side (RHS) of linear system (19).

Normalization factor utilized in the OpenFOAM® represents so called $\mathbf{L_1}$ norm. Skewed cell produce an artificially high rate of the RHS source terms, hereby decreasing residuals level to the under-estimated one. Thus a linear solver detects that convergence criterion is already reached and the iteration process is stopped.

Possible solutions are either to modify the OpenFOAM® libraries to utilize proper normalization, which is not prone to similar error, or to set the residuals level in solution control dictionary to the artificially strict level of 10^{-14}~10^{-12}, and restrict maximum number of the iterations along with the high relative tolerance 10^{-3}~10^{-2}. The latest means that we improve the solution accuracy by 2-3 orders of the magnitude.

The revised results using the adjusted convergence criterion for the turbulent flow simulation are presented in Fig. 3. A more smooth distribution of the calculated quantities is observed indicating a high turbulent mixing. All equations of the model are consequently solved and no "freezing quantity" occurs. It doesn't show the highly resolved eddy structures any more, as what we have seen in Fig. 2, but the numerical solution is correct according to the RANS model hypothesis of the averaged instantaneous velocity oscillations. On this base the small vortices are not detected within the frames of RANS, however granting enough information of the transient turbulent flow for further solidification modeling.

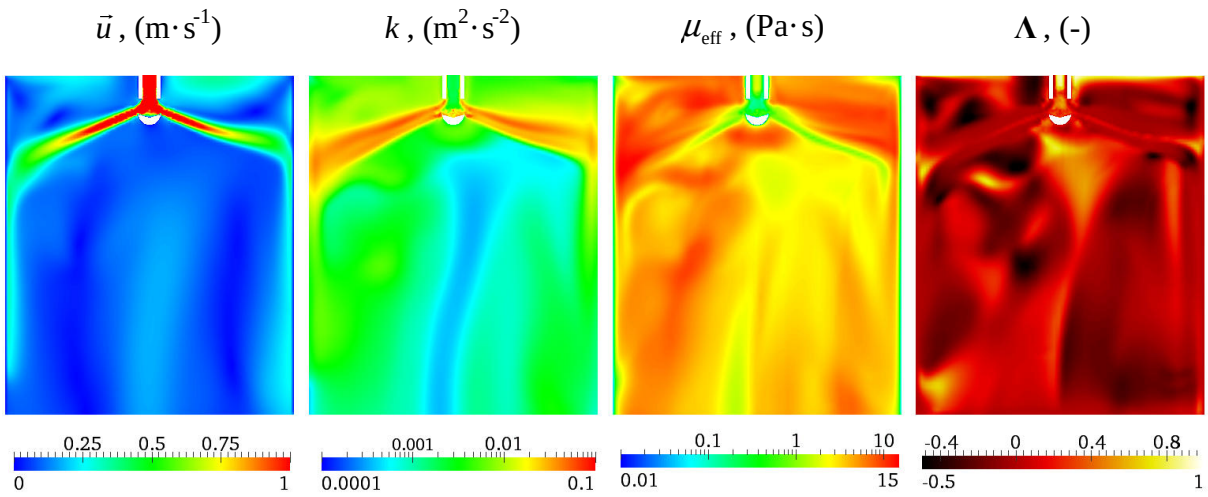

Figure 3. Flow pattern in the CC mold for the case of the enhanced convergence settings: (a) velocity field; (b) turbulent kinetic energy; (c) effective viscosity; (d) flow type function.

Additionally it is possible to correct some errors for the $k-\varepsilon$ transport, which are connected with the inaccuracy in the solution of the continuity equation (1). Conservative form of the convectional term in Eq. (5) is

$$\nabla\cdot\left(\rho\vec{u}k\right)=\rho\nabla\cdot\left(\vec{u}k\right). \tag{28}$$

Induced incompressibility correction can be expressed as

$$\vec{u}=\vec{u}^{*}+\boldsymbol{\delta}\quad\Rightarrow\quad\vec{u}^{*}=\vec{u}-\boldsymbol{\delta}, \tag{29}$$

where $\vec{u}^{*}$ represents the exact solution, $\vec{u}$ is the calculated one and $\boldsymbol{\delta}$ is an error vector. The exact solution $\vec{u}^{*}$ fulfils the continuity equation (1), thus

$$\nabla\cdot\vec{u}^{*}=0\quad\Rightarrow\quad\nabla\cdot\vec{u}=\nabla\cdot\vec{u}^{*}+\nabla\cdot\boldsymbol{\delta}=\nabla\cdot\boldsymbol{\delta}. \tag{30}$$

So if it would be possible to get the exact solution at each of iterations, a gradient form could be written for Eq. (28) omitting the constant density in the expression:

$$\nabla\cdot\left(\vec{u}^{*}k\right)=\vec{u}^{*}\vec{\nabla}k. \tag{31}$$

Next according to Eq. (29) the calculation error is estimated:

$$Err=\nabla\cdot\left(\vec{u}k\right)-\vec{u}^{*}\vec{\nabla}k=k\nabla\cdot\vec{u}^{*}+\vec{u}^{*}\vec{\nabla}k+k\nabla\cdot\boldsymbol{\delta}+\boldsymbol{\delta}\vec{\nabla}k-\vec{u}^{*}\vec{\nabla}k. \tag{32}$$

Applying Eq. (30) we get

$$Err=k\nabla\cdot\boldsymbol{\delta}+\boldsymbol{\delta}\vec{\nabla}k=k\nabla\cdot\vec{u}+\boldsymbol{\delta}\vec{\nabla}k. \tag{33}$$

Thereby performing a correction for the convectional term in the form

$$\nabla \cdot \left(\bar{u}^{*} k \right) \approx \nabla \cdot \left(\bar{u} k \right) - k \nabla \cdot \bar{u} \tag{34}$$

the incompressibility estimation error is reduced to $\boldsymbol{\delta} \vec{\nabla} k$.

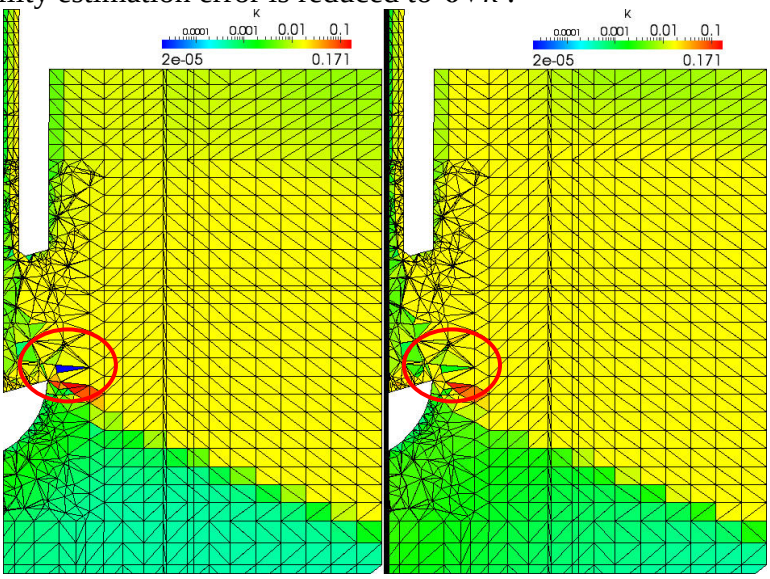

a) b)

Figure 4. Turbulent energy k distribution calculated using advection term in (a) the divergent form and (b) with the incompressibility correction.

Described correction approach was tested and approved for the transport of turbulent quantities on the unstructured grids. As an example, in Fig. 4(a) one can see the calculated distribution of the turbulent kinetic energy at the SEN port region. The highest values are detected at the sharp edge of the port where the most turbulence is generated. However the artificially low k value is detected for the highly skewed mesh element (blue color in the marked area). After applying the convection term correction, error value is vanished and more smooth distribution of the k field is observed (see Fig. 4(b)).

4. MESH REFINEMENT FOR SOLIDIFICATION FRONT TRACKING

Traditionally mesh refinement is performed by introducing boundary layers (BL) at the high gradient regions e.g. near walls and phase interfaces. Utilization of the BL is also a well known technique to treat the laminar sublayer of the turbulent flow. However this mesh is static and does not track the transient behavior of the considered phenomenon.

During solidification simulation of the continuous casting it was observed that a solid shell thickness is under-estimated if compared to the reality. Extension of the boundary layer produces more accurate simulation results within the solidifying region, but is an inefficient approach, because it guides to the enormous number of cells, considerable part of which is in the totally solidified region, where the high mesh resolution is actually not necessary.

To find a proper mesh refinement method it is necessary to study the correlation between the solid phase fraction and the temperature [1, 13]:

$$f_s = \begin{cases} 0 & T \geq T_{\text{liquidus}}, \\ 1-((T_{\text{f}}-T)/(T_{\text{f}}-T_{\text{liquidus}}))^{1/(k_{\text{p}}-1)} & T_{\text{liquidus}} > T > T_{\text{eutectic}}, \\ 1 & T_{\text{eutectic}} \geq T. \end{cases} \tag{35}$$

One can see that the relation of Eq. (35) is noticeably non-linear. For instance, it is desired to have at least 10 grid points within the mush zone. We can either intend to track the solid fraction (Fig. 5(a)) with the regular stepping between resolved values within the BL or rely upon the temperature distribution (Fig. 5(b)). Respectively the grid points in the appropriated boundary layers are mapped in Fig. 6. Generally it should be noted that the 100% solid represents the wall surface and adjacent regions if the shell thickness increases.

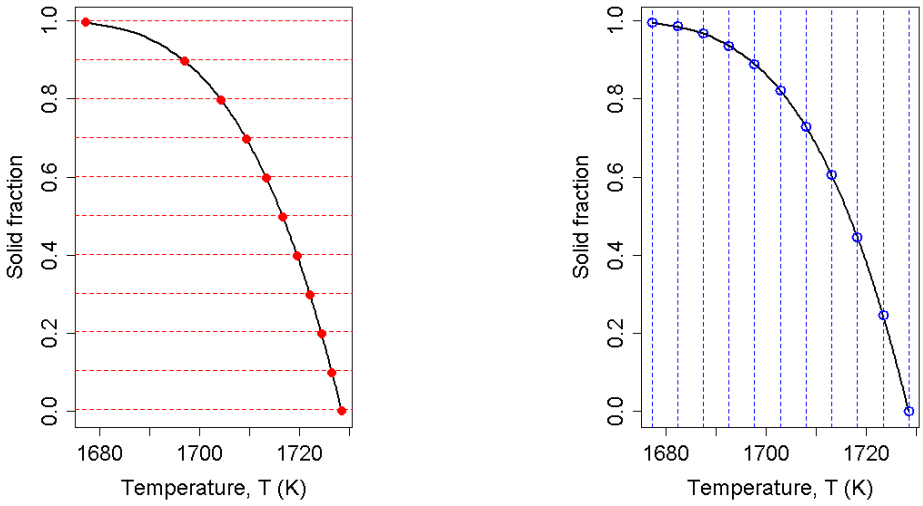

a) b)

Figure 5. Scheil curve for the $f_s - T$ correlation:
(a) regular f_s stepping and (b) regular T stepping.

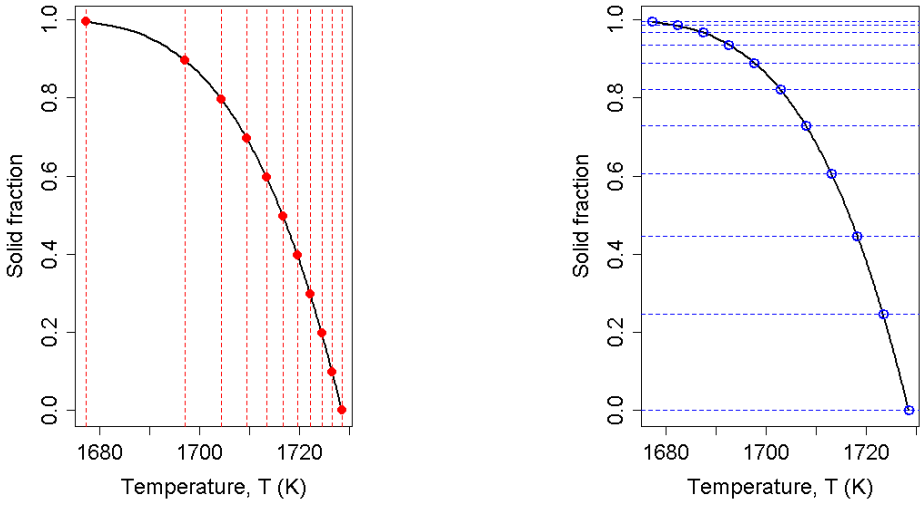

a) b)

Figure 6. Grid points density according to (a) f_s stepping and (b) T regular stepping.

If the solid fraction is used as the refinement factor, the temperature is better resolved at the starting point (solidification front) of the two phase region (Fig. 6(a)). However there is lack

of accuracy for its prediction near the walls where the most temperature gradients are observed due to the contact with the chill. If the meshing procedure is aimed to improve the temperature distribution, there is an issue with the proper calculation of the phase fraction because of the insufficient number of the grid points within the mush zone. They are mostly concentrated in the vicinity of the 100%-solid surface (Fig. 6(b)) where the solid shell is already formed and no medium motion occurs apart of the pulling process.

Thereby it is necessary to have a compromise for the grid adjustment, taking into account the fact that the number of mesh cells after refinement is limited by the computer hardware resource. In the current work a static method was used for the grid refinement. First of all, a coarse mesh was used with the introduced BL merely at the chill walls using third party meshing tool (Fig. 7(a)). As the next step, several refinements were done by means of the *refineMesh* tool according to some semi-empirical criteria for the cells with the most difference in the solid phase and temperature distributions. Additionally a limiting of the refinement only in the lateral direction was applied.

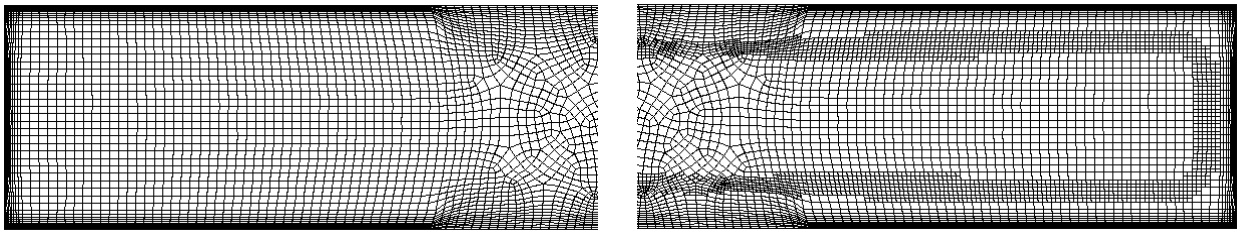

a) b)

Figure 7. Numerical grid for the solidification solver:
(a) initial one created with the Gambit BL;
(b) after the refinement with the OpenFOAM® tool

A mesh refinement procedure was repeated serially each time when the coarser grid solution has reached the quasi-steady state (e.g. a certain shell thickness was obtained). Corresponding results are shown in Fig. 7(b).

5. BOUNDNESS AND ACCURACY OF THE HEAT TRANSFER CALCULATION

During the numerical studies of the solidification processes with the designed solidification solver [17-18] it was detected that a temperature over-estimation occurred. It leads to the unwanted side effects, such as the remelting due to the increased ‘superheat’ being brought to the solidified region. In accordance with the performed discretization analysis, the energy equation Eq. (14) was proved to be a source of wrong temperatures. It was also revealed that the same behavior occurred even without taking into account the solidification (Fig. 8).

Let’s consider transport equation for the temperature

$$\frac{\partial T}{\partial t} + \nabla \cdot \left(\vec{u} T \right) = \nabla \cdot \kappa_{\text{eff}} \vec{\nabla} T \,, \tag{36}$$

where $\kappa_{\text{eff}} = \dfrac{\alpha_{\text{eff}}}{\text{c}_\text{p} \rho}$ represents effective thermal diffusivity.

Next, Eq. (36) is split into convectional and diffusive parts:

$$\frac{\partial T}{\partial t} + \nabla \cdot \left(\vec{u} T \right) = 0 \,, \tag{37}$$

$$\frac{\partial T}{\partial t} - \nabla \cdot \kappa_{\text{eff}} \nabla T = 0 . \qquad (38)$$

Above Eq. (37)-(38) are solved together with the Navier-Stokes equations for the flow and turbulence. The same heat flux boundary condition as for the solidification modeling is used. After the turbulent flow and heat transfer are developed, the analysis of the temperature field is carried out. Observations indicated that the estimation of the temperature overshoots $\Delta^{T}_{\text{error}} = T_{\max} - T_{\text{tundish}}$ exceeded 560 K for the convection equation (37), whereas for the diffusive one according to Eq. (38) the violation level remained insignificant. Therefore, the discretization procedure of the convectional part of the energy equation is most critical and should be improved to ensure physically correct result.

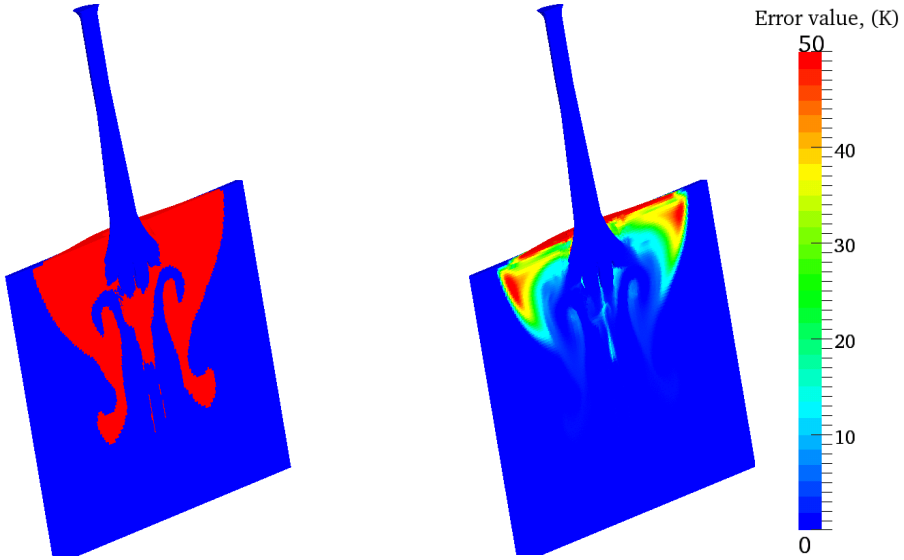

a) b)

Figure 8. Volume elements with (a) error values (marked with red) and (b) the scaled temperature overshoots.

It is known [20] that all convectional schemes can be categorized in two groups: those, which guarantee and maintain the boundness of the numerical solution, and those, which provide higher precision of discretization. Schemes of the first category are mostly of the low accuracy and introduce considerable level of the numerical diffusion. Hereupon it becomes impossible to trace the strong gradients of the solution, which are artificially smoothed.

Convectional schemes of the second category are prone to the spurious oscillations of the numerical solution and quite often produce unphysical results. On the one hand such behavior can be relatively easy detected for the scalar transport problems with the well know variation range. On the other hand, when minimum and maximum values are not fixed or some gradient boundary conditions are applied, a question regarding validation criterion arise.

Due to lack of a simultaneously bounded and accurate scheme, a compromise should be found. Usually TVD and NVA approaches are used to combine stability, boundness and accuracy for the discretization procedure.

To verify the numerical behavior of the convectional schemes implemented in the OpenFOAM CFD software a stationary transport equation was solved:

$$\nabla \cdot \left(\phi \vec{u} \right) = 0 , \qquad (39)$$

where ϕ is a passive scalar. A simulation domain of the benchmark is a 2D square (Fig. 9). Left and bottom sides correspond to the inlet, right and top are the outlet boundaries. Step profile of the scalar ϕ brought by the flow from the left is defined as

$$\phi = \begin{cases} 0 \quad \text{for} \quad 0 \le x < \dfrac{1}{6}, \\ \\ 1 \quad \text{for} \quad \dfrac{1}{6} \le x \le 1. \end{cases} \tag{40}$$

Right and the left boundaries are set to the zero gradient condition.

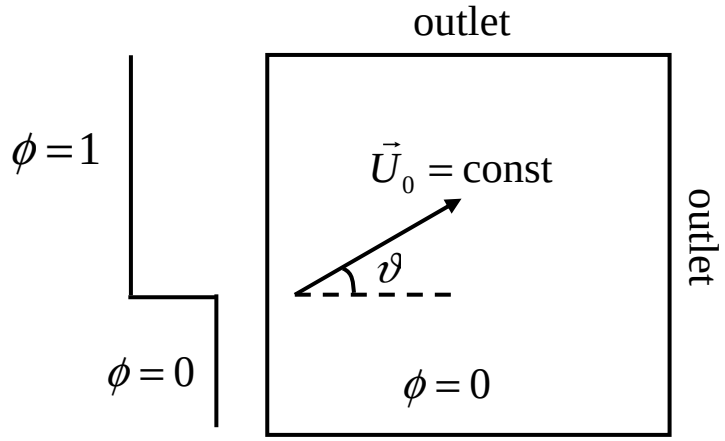

Figure 9. Initial setup of the 2D benchmark for testing the convectional schemes.

To simplify the interpretation of the test results velocity represents a unit vector with the fixed mesh-to-flow angle, $\vartheta = 30^\circ$. Numerical grid is uniformly spaced and consists of 30×30 control volumes. Comparison between the analytical and the numerical solutions of the transport equation Eq. (39) is made across the vertical line, which is 20 CV downstream from the left inlet boundary. The exact solution in this case is

$$\phi\big|_{x=\frac{2}{3}} = \begin{cases} 0 \quad \text{for} \quad 0 \le y < \dfrac{4+\sqrt{3}}{6\sqrt{3}}, \\ \\ 1 \quad \text{for} \quad \dfrac{4+\sqrt{3}}{6\sqrt{3}} \le y \le 1. \end{cases} \tag{41}$$

As provided by the analytical solution, the transported step profile should remain sharp. Hereby, the behavior of the numerical schemes is evaluated according to following criteria: diffusivity of the scheme (how the sudden change of the solution is smeared due to the lack of discretization accuracy) and the ability of the scheme to keep the physical boundaries of the transported scalar.

According to advanced application practice the upwind differencing (UD), central differencing (CD), linear-upwind differencing (LUD [21]), self-filtered central differencing (SFCD [22]) and the Gamma [20] schemes were tested and compared. Figs. 10-15, representing the test results, contain the color map (left) of the simulated scalar along with the comparison plot of the exact and modeled profiles at the position 20 CVs downstream from the left boundary (top-right) and the numerical error distribution pattern (bottom-right).

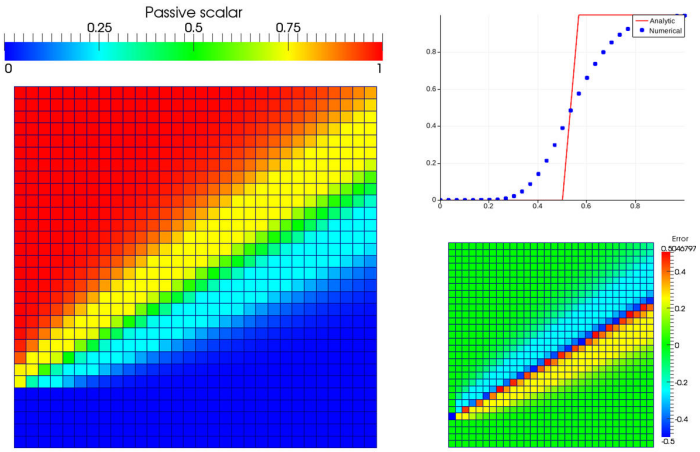

Figure 10. Simulation results of a passive scalar transport (UD scheme)

The upwind differencing (UD) scheme provides the most bounded solution without any additional numerical tricks due to its physical nature, resulting in the strongly smoothed step profile though (Fig. 10). Thus UD scheme is too diffusive and, despite it conserves scalar being transported within desired range, it can not tackle the strong gradient (which occur rather often during solidification processes). UD can be widely used for the starting period of the simulation procedure to stabilize it.

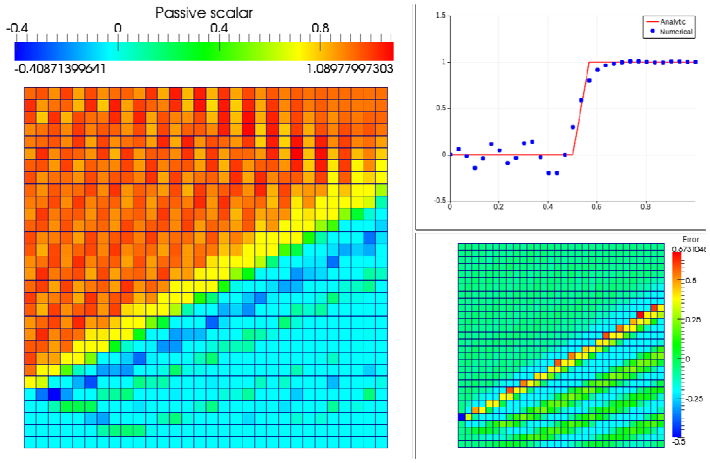

Figure 11. Simulation results of a passive scalar transport (CD scheme)

Central differencing (CD) scheme is more accurate and follows the sudden change of the simulated value (Fig. 11). However it produces spurious oscillations of the numerical solution up- and downstream. Thus a positive scalar can reach negative values as well as overshoots of the solution are observed.

Linear upwind differencing (LUD) scheme is designed to take advantages of both UD and CD. It combines the boundness of the former and brings the accuracy of the latter. However according to the test results it still produces small under- and overshoots of the solution (Fig. 12).

To exclude the unboundedness of the numerical solution, a cell / face limiting of the gradient is applied either between the neighboring volumes or at the interface between them. Such procedure is aimed to avoid unphysical peaks of the calculated gradients between the cells. After cell / face correction is applied one can observe that LUD scheme tracks both the sharpness of the step profile and the boundness of the simulated value (Fig. 13).

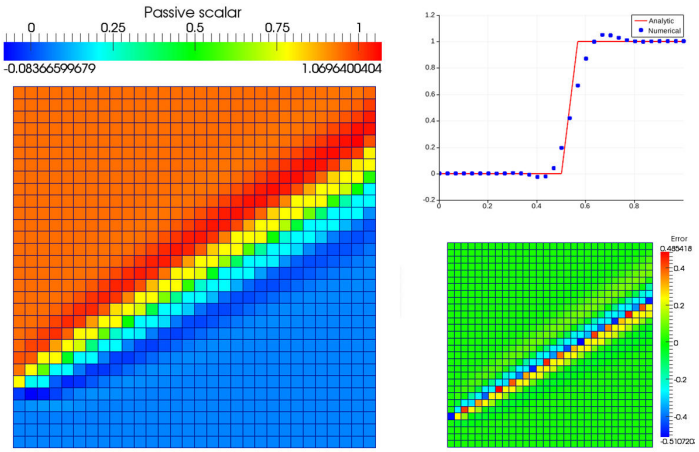

Figure 12. Simulation results of a passive scalar transport (LUD scheme)

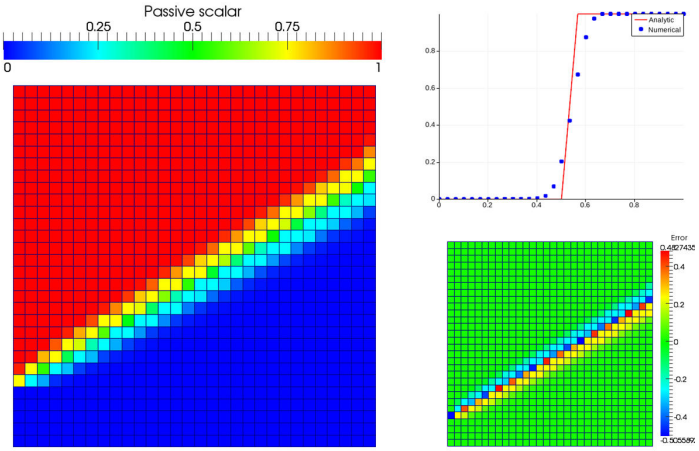

Figure 13. Simulation results of a passive scalar transport (LUD scheme with cell limiting)

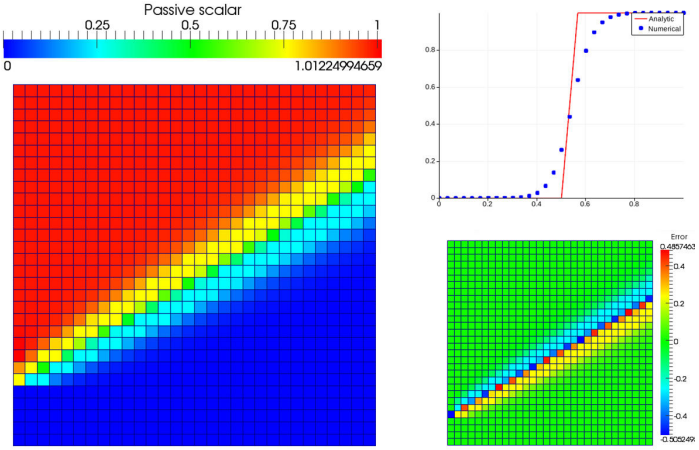

Figure 14. Simulation results of a passive scalar transport (SFCD scheme with cell limiting)

The similar tests were carried out for the SFCD and the Gamma schemes. One can see the results (Fig. 14 and Fig. 15) with cell limiting been applied. As opposed to LUD scheme both of them lead to some overshoots ~1% of the maximum value at the step profile and seem to be a little bit more diffusive than LUD one.

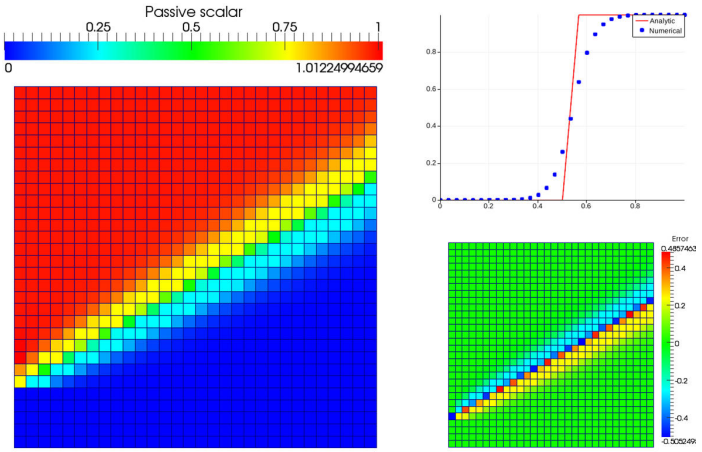

Figure 15. Simulation results of a passive scalar transport
(Gamma scheme with cell limiting)

Based on the above analyses linear-upwind differencing scheme was proposed for the discretization of the convectional term, together with the cell limiting of the gradients. Both supplements of the initial algorithm were proved to be effective to maintain the boundness of the solution.

6. NON-LINEARITY OF THE MODEL

It was already mentioned that the coupling between the turbulent flow and solidification is strongly non-linear. A latent heat recovery method led to the segregated approach for the solidification solver (Fig. 16). Thereby all the equations are solved sequentially utilizing an under-relaxation procedure for updating the porous resistance and heat source terms. Under-relaxation method is known as a reliable tool for the non-linear problems; however it is characterized by the significant number of the internal iteration loops of the solution algorithm, especially for the transient tasks.

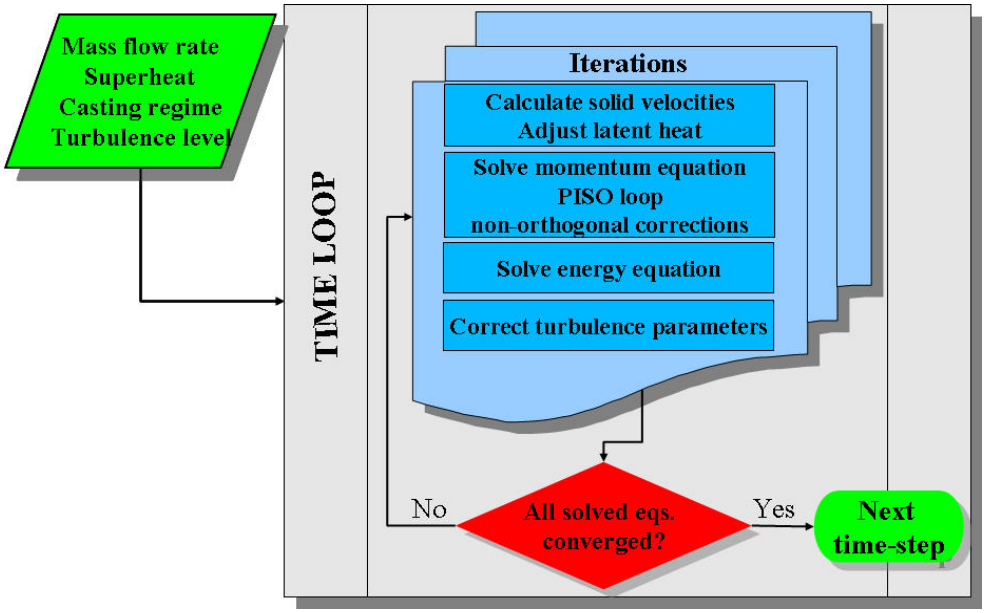

Figure 16. Flow chart of the solution algorithm.

One can evidently observe how the number of the iterations drastically increases with the relaxation parameter decrease (Fig. 17). Some solidification simulations require the under-

relaxation factor ω as small as 0.05. It implies that each time step of the calculation might need as much as 100-200 steps to get the solution converged. A typical solidification simulation would run for weeks on the relatively powerful hardware.

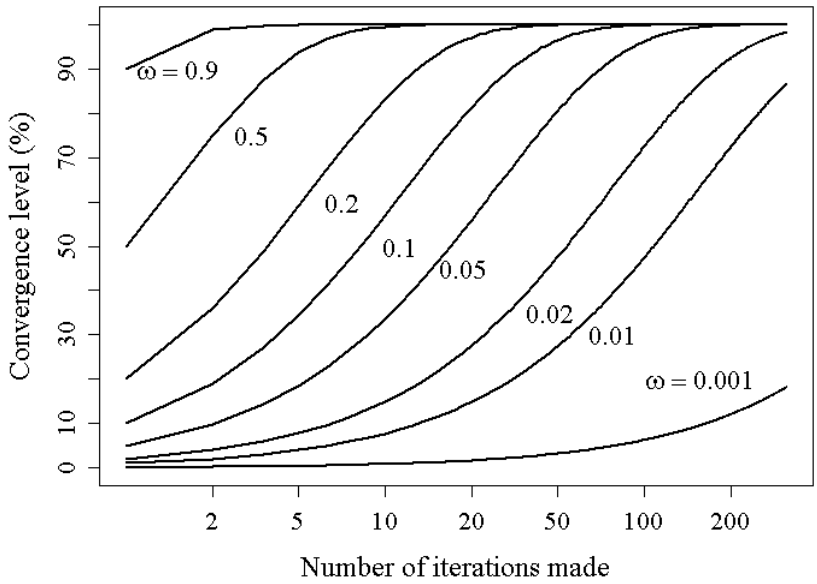

Figure 17. Convergence behavior of the under-relaxation procedure

The ongoing work is devoted to make use of the full capacity of the OpenFOAM® extended version [23] to deal with the block-matrix methodology for the strongly coupled PDE systems. It permits to avoid the additional iteration process for coupling and improve the convergence rate.

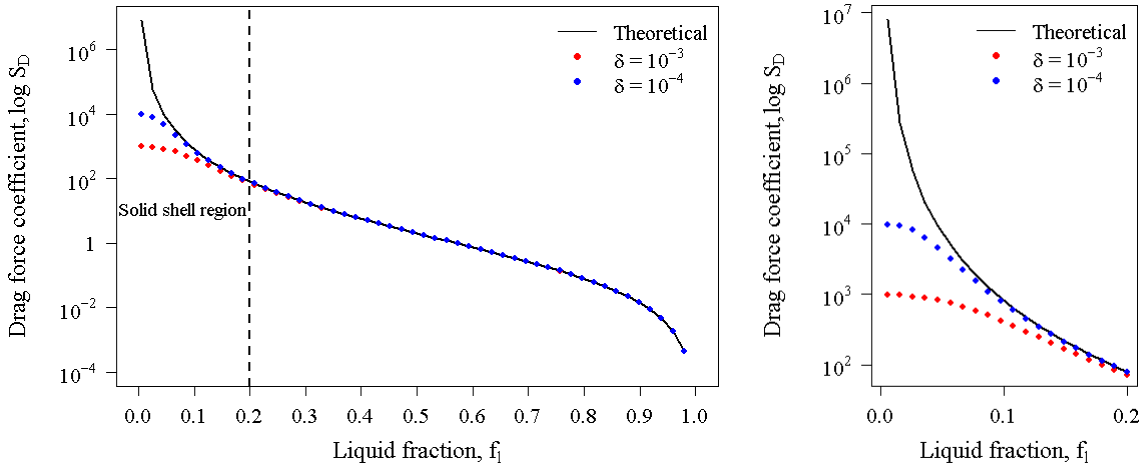

a) b)

Figure 18. Drag force coefficient as function of liquid volume fraction:
a) whole two-phase region; b) near the end of solidification.

Another issue of non-linearity is related to the permeability law of porous media being used in the model. Previous studies [1] have shown that due to the high porous resistance of the two phase region a melt flow can only penetrate into the mush as deep as $f_s = 20 \sim 30\%$. The porous resistance, here also named as drag force coefficient, can be evaluated by inverting Eq. (4):

$$\frac{1}{K} = \frac{f_s^{\,2}}{f_l^{\,3} + \delta} \cdot \frac{1}{6 \cdot 10^{-4} \cdot \lambda_1^2}, \tag{42}$$

where δ, according to the FLUENT® User Guide [19], is a small number in the magnitude of $10^{-4} \sim 10^{-3}$. A question arises if the δ value influences the permeability dramatically. This comes really into effect, e.g. for some steel grades where minimal liquid fraction, remaining in the mush, is $\sim 5 \times 10^{-3}$. The term $f_l^{\,3} \sim 10^{-6}$ is actually 2 orders of the magnitude smaller than δ in the pre-factor $\frac{f_s^{\,2}}{f_l^{\,3} + \delta}$.

Performed studies have shown (Fig. 18) that the difference of drag coefficients due to different δ, as calculated by Eq. (42), takes only effect for the liquid fraction lower than 20 %. At this stage of solidification the liquid melt is almost solidified and there is no significant convection. Therefore, the assumed numerical form of the permeability law does not affect the final simulation result of solidification. On the contrary it helps to enhance the stability and the convergence rate of the numerical solution by reducing the difference in the matrix diagonal coefficient and bounding the porous resistance to a reasonable range.

7. SUMMARY DISCUSSIONS

In this work a numerical model considering turbulent flow and solidification is implemented in the OpenFOAM® CFD software. The treatment of the solidification latent heat considering the relative motion of the dendritic structures of the continuous casting with the complex mold geometries (curvature of the mold) is improved. Based on the Eulerian formulation of the energy equation a proper form of the latent heat advection term is considered.

In the framework of the RANS approach the turbulence transport quantities, k and ε, are analyzed. The convergence criterion for both k and ε transport equations was adjusted based on the analyses of the residual normalization. The incompressibility corrections for the convectional terms in the k and ε equations are investigated and approved.

A static mesh refinement method is utilized to improve the prediction of the solid shell formation. The on-going developments are devoted to the dynamic mesh adjustment, i.e. automatic refinement and coarsening during the calculation.

A number of the convectional schemes, which have been implemented in the OpenFOAM® CFD software, are checked with regard to the accuracy and boundness of the numerical solution. It is found that the face or cell limiting of the gradient calculation is required for the convectional term in the energy equation to avoid the spurious oscillations of the numerical solution. Hereby the evaluation of the temperature field using unstructured numerical grid is made, and the heat transfer part of the solidification model is improved.

The under-relaxation procedure in the frame of the segregated approach is considered to enhance the coupling efficiency of the fluid flow with the evolution of the two-phase region. On the one hand it is claimed to be rather stable; on the other hand the under-relaxation procedure is proved to be inefficient and computational-time consuming one. The fully coupled solution using the new block-matrix library and solver of the OpenFOAM® extended version is supposed to be a new alternative for the strongly coupled problems such as the solidification. It is significant for the non-linear latent heat adjustment formulation and also for the complex permeability law of the two phase region as well.

ACKNOWLEDGEMENT

The financial support by RHI AG, the Austrian Federal Ministry of Economy, Family and Youth and the National Foundation for Research, Technology and Development is gratefully acknowledged. The authors acknowledge the fruitful discussions of the numerical algorithms with Prof. Karl Kunisch, University of Graz, Austria.

NOMENCLATURE

c_p	$J \cdot kg^{-1} \cdot K^{-1}$	specific heat
$C_{1\varepsilon}, C_{2\varepsilon}, C_\mu$	[-]	constant of the standard $k-\varepsilon$ model
f_ℓ, f_s	[-]	volume fraction of liquid and solid phase
G	$kg \cdot m^{-1} \cdot s^{-3}$	shear production of turbulence kinetic energy
h	$J \cdot kg^{-1}$	enthalpy
h_{ref}	$J \cdot kg^{-1}$	reference enthalpy at temperature T_{ref}
k	$m^2 \cdot s^{-2}$	turbulence kinetic energy per unit of mass
K	m^2	permeability
L	$J \cdot kg^{-1}$	latent heat
p	$N \cdot m^{-2}$	pressure
$Pr_{t,k}$	[-]	Prandtl number for turbulence kinetic energy k
$Pr_{t,\varepsilon}$	[-]	Prandtl number for turbulence dissipation rate ε
S_k	$kg \cdot m^{-1} \cdot s^{-3}$	source term for turbulence kinetic energy
S_ε	$kg \cdot m^{-1} \cdot s^{-4}$	source term for turbulence dissipation rate
$\vec{S}_D$	$kg \cdot m^{-2} \cdot s^{-2}$	source term for momentum equation
t	s	time
T	K	temperature
T_{ref}	K	reference temperature for h_{ref}
T_f	K	melt point of pure solvent
$T_{eutectic}$	K	temperature of eutectic reaction
$T_{liquidus}$	K	liquidus temperature of alloy
$\vec{u}$	$m \cdot s^{-1}$	velocity of the mixture
$\vec{u}_\ell$	$m \cdot s^{-1}$	liquid velocity
$\vec{u}_s$	$m \cdot s^{-1}$	solid velocity
ε	$m^2 \cdot s^{-3}$	turbulence dissipation rate per unit of mass
α	$W\ m^{-1} \cdot K^{-1}$	thermal conductivity
α_{eff}	$W\ m^{-1} \cdot K^{-1}$	effective thermal conductivity due to turbulence
α_t	$W\ m^{-1} \cdot K^{-1}$	turbulence thermal conductivity
λ_1	m	primary dendrite arm spacing
ρ	$kg \cdot m^{-3}$	density
μ_{eff}	$kg \cdot m^{-1} \cdot s^{-1}$	dynamic effective viscosity due to turbulence
μ_ℓ	$kg \cdot m^{-1} \cdot s^{-1}$	dynamic liquid viscosity
μ_t	$kg \cdot m^{-1} \cdot s^{-1}$	dynamic turbulence viscosity

REFERENCES

1. M. Wu, A. Vakhrushev, G. Nummer, C. Pfeiler, A. Kharicha and A. Ludwig, “Importance of Melt Flow in Solidifying Mushy Zone”, *Open Transport Phenomena J. – Bentham Open*, vol. 2, pp. 16-23, 2010.
2. C. Pfeiler, “Modeling of Turbulent Particle/Gas Dispersion in the Mold Region and Particle Entrapment into the Solid Shell of a Steel Continuous Caster”, PhD thesis, Montanuniversität Leoben (2008).
3. M. Rappaz, “Modelling of Microstructure Formation in Solidification Processes”, *Intern. Mater. Rev.*, vol. 34, Issue 3, pp. 93-123, 1989.
4. C. Beckermann, and R. Viskanta, “Mathematical modeling of transport phenomena during alloy solidification”, *Appl. Mech. Rev.*, vol. 46, pp.1-27, 1993.
5. V.R. Voller, and C. Prakash, “A fixed grid numerical modeling methodology for convection – diffusion mushy region phase-change problems”, *Int. J. Heat Mass Transfer*, vol. 30, No. 8, pp. 1709-1719, 1987.
6. V.R. Voller, A.D. Brent, and C. Prakash, “The modeling of heat, mass and solute transport in solidification systems”, *Int. J. Heat Mass Transfer*, vol. 32, No. 9, pp. 1719-1719, 1989.
7. V.R. Voller, A.D. Brent, and C. Prakash, “Modeling the mushy region in a binary alloy”, *Appl. Math. Modeling*, vol. 14, pp. 320-326, 1990.
8. V.R. Voller, and C.R. Swaminathan, “General source-based method for solidification phase change”, *Numerical Heat Transfer*, Part B, vol. 19, pp. 175-189, 1991.
9. P.J. Prescott, and F.P. Incropera, “The effect of turbulence on solidification of a binary metal alloy with electromagnetic stirring”, in: *Transport Phenomena in Materials Processing and Manufacturing*, ASME HTD, vol. 280, pp. 59-69, 1994.
10. P.J. Prescott, and F.P. Incropera, “Convective transport phenomena and macrosegregation during solidification of a binary metal alloy: I-Numerical predictions”, *J. Heat Transfer*, vol. 116, pp. 735-741, 1994.
11. P.J. Prescott, F.P. Incropera, and D.R. Gaskell, “Convective transport phenomena and macrosegregation during solidification of a binary metal alloy: II-Experiments and comparisons with numerical predictions”, *Trans. ASME*, vol. 116, pp. 742-749, 1994.
12. P.J. Prescott, and F.P. Incropera, “The effect of turbulence on solidification of a binary metal alloy with electromagnetic stirring”, *Trans. ASME*, vol. 117, pp. 716-724, 1995.
13. Dantzig, J. A, and Michel Rappaz. *Solidification*. 1. ed.: EPFL Press, 2009.
14. Rhie, C.M. and Chow, W.L., “A numerical study of the turbulent flow past an isolated airfoil with trailing edge separation”, AIAA-82-0998, AIAA/ASME 3rd Joint Thermophysics, Fluids, Plasma and Heat Transfer Conference, St. Louis, Missouri, 1982.
15. Perić, M., “A Finite Volume method for the prediction of three-dimensional fluid flow in complex ducts”, PhD thesis, Imperial College, University of London, 1985.
16. J.P. Gu,and C. Beckermann, “Simulation of convection and macrosegregation in a large steel ingot”, *Metall. Mater. Trans. A*, vol. 33A, pp.1357-1366, 1999.
17. A. Vakhrushev, A. Ludwig, M. Wu, Y. Tang, G. Nitzl, G. Hackl: Modeling of Turbulent Melt Flow and Solidification Processes in Steel Continuous Caster with the Open Source Software Package OpenFOAM; OSCIC’10 Conf., Munich, 2010
18. A. Vakhrushev, A. Ludwig, M. Wu, Y. Tang, G. Nitzl, G. Hackl: Modeling of Heat Transfer and Solidification Processes in Thin Slab Caster, 4th Int. Conf. Simulation and

Modeling in Metallurgical Processes in Steelmaking (STEELSIM 2011) Düsseldorf, Germany, June 27 – July 01 (2011)
19. Fluent: *FLUENT 6.3 User's Guide*, Fluent Inc. (2006).
20. H. Jasak, H.G. Weller, A.D. Gosman: High resolution NVD differencing scheme for arbitrarily unstructured meshes; Int. J. Num. Methods in Fluids, vol. 31, pp. 431-449, 1999
21. R.F. Warming; et al.: Upwind second-order difference schemes and applications in aerodynamic flows; AIAA J., vol. 14, pp. 1241–1249, 1976
22. STAR-CD Manuals v2.1; Comp. Dynamics, 1991
23. The OpenFOAM®-Extend Project: Community-driven Releases of OpenFOAM®. http://extend-project.de